# Quantum effects in light and heavy liquid water: A rigid-body centroid molecular dynamics study

L. Hernández de la Peña and P. G. Kusalik
*Department of Chemistry, Dalhousie University, Halifax, Nova Scotia B3H 4J3, Canada*

(Received 12 April 2004; accepted 24 June 2004)

The centroid molecular dynamics (CMD) method is applied to the study of liquid water in the context of the rigid-body approximation. This *rigid-body CMD* technique, which is significantly more efficient than the standard CMD method, is implemented on the TIP4P model for water and used to examine isotopic effects in the equilibrium and dynamical properties of liquid $H_2O$ and $D_2O$. The results obtained with this approach compare remarkably well with those determined previously with path integrals simulations as well as those obtained from the standard CMD method employing flexible models. In addition, an examination of the impact of quantization on the rotational and librational motion of the water molecule is also reported. © *2004 American Institute of Physics.* [DOI: 10.1063/1.1783871]

## I. INTRODUCTION

Methods based on Feynman's path integral representation of statitistical mechanics[1] have been extensively used to calculate equilibrium properties of systems in condensed phase.[2–6] Liquid water, in particular, has benefited from the progress made in this area and a number of path integrals simulations has been reported to date. Kuharsky and Rossky[3] performed equilibrium path integral Monte Carlo (PIMC) simulations on the rigid and nonpolarizable ST2 (Ref. 7) water model and they concluded that the structural changes due to quantum effects were equivalent to rising the temperature by ≈50 K. Wallqvist and Berne[4] used path integral molecular dynamics (PIMD) to study a flexible central force model and found similar quantum structural effects. The PIMD method was later used by del Buono and Rossky[5] to calculate the quantum isotope effect on other rigid models [ST2, SPC (Ref. 8), and TIP4P (Ref. 9)] and similar results were again obtained. More recently, Stern and Berne[6] studied liquid $H_2O$ via PIMD using a flexible water model parametrized from *ab initio* calculations and reported that the quantum liquid is less structured and has smaller binding energies than the classical liquid, in accord with previous simulations. A far more ambitious equilibrium calculation has been very recently performed by Chen and co-workers[10] using a Car-Parinello path integral molecular dynamics method. Interestingly, the results from this work indicate that the previously identified ''softening'' of the intermolecular interactions may be at least partially overcome by an increase of the molecular dipole moment, that arises, reportedly, when quantum effects in the motion of both nuclei and electrons are simultaneously included.

Within a computer simulation, approximate quantum dynamical information has also become available through the centroid molecular dynamics (CMD) methodology.[11] This methodology, while reproducing the already known equilibrium properties, also allows the calculation of (approximate) quantum time-dependent properties. It is particularly accurate in systems with behavior close to the classical limit. Using this technique, Lobaugh and Voth[12] modified a simple point charge flexible water model and determined estimates for the equilibrium and dynamical properties of quantum water. They found that quantum time correlation functions decay faster than the corresponding classical ones, consistent with the expected tunneling behavior in liquid water.[3,12] Equilibrium and dynamical behavior have also been extracted for light and heavy water at different temperatures with the use of an effective potential technique,[13] based on the Feynman-Hibbs variational treatment; the results agree reasonably well with the more accurate but computationally more expensive CMD method.

Although both rigid and flexible water models have been used to simulate liquid water, it is well known that most bulk properties are very well reproduced without the inclusion of molecular vibrations.[14] Very recently, first-principles simulations of rigid water[15] have been found to reproduce experimental results well, while the inclusion of flexibility in the water model appeared to impact negatively on this agreement. Furthermore, quantum simulations on rigid models[3,5] have confirmed that more than 90% of the effects of quantization appear to be due to the orientational degrees of freedom, which can be easily seen as a consequence of the fact that the water molecule has small inertia moments but a relatively large total mass. Thus, the purpose of this work is to report results on light and heavy water obtained using the centroid molecular dynamics methodology adapted within the context of the rigid-body approximation. The advantage of this approximation in relation to the standard CMD method is that the number of degrees of freedom required in the simulation is decreased significantly; classically by excluding the vibrational motion, and quantum mechanically by the use of a significantly lower value of the discretization parameter $P$ (due to the rigid rotor treatment of the molecule). As a consequence, the simulation is more than 20 times more efficient (per unit of real time simulated) than the original CMD while still performing an evaluation of the centroid forces (and centroid torques) according to the local

 

molecular environment. It is interesting to point out that the Feynman-Hibbs effective potential technique is, however, still much faster at the expense of the assumption of a specific form for the (temperature dependent) effective potential, which is in turn an approximation to the CMD centroid potential. In a future study we will report results exploring the validity of this ''local environment independent'' approximation in the effective potential.

The present study, through a direct comparison with previous simulation results, addresses the relevance of rigid models in the calculation of bulk properties within a quantum simulation of liquid water. This paper is organized as follows. Section II reviews the Cartesian CMD methods and describes its extension to rigid bodies. Section III presents the details of the simulation methodology and a number of parametrization tests. In Sec. IV we present our simulation results and discuss the impact of the quantum mechanical uncertainty in equilibrium and dynamical properties of liquid $H_2O$ and $D_2O$. Our conclusions are given finally in Sec. V.

## II. COMPUTATIONAL METHODS

### A. The CMD method

In the Feynman's formulation of statistical mechanics[1] (i.e., in terms of imaginary time path integrals) the partition function is a sum of weighted exponents of the imaginary time action over all closed paths, i.e.,

$$Z=\int \rho(x,x;\beta)dx=\int_{x(0)=x(\beta\hbar)}\mathcal{D}x(\tau) \times\exp\left\{-\frac{1}{\hbar}S[x(\tau)]\right\}, \tag{1}$$

where

$$S[x(\tau)]=\int_0^{\beta\hbar}\left\{\frac{m}{2}\frac{dx(\tau)}{d\tau}+V[x(\tau)]\right\}d\tau \tag{2}$$

is the Euclidean action functional. In the above equations $\rho(x,x;\beta)$ is the diagonal element of the thermal density in the coordinate representation, $\beta$ is the inverse of temperature in units of energy, $\int_{x(0)=x(\beta\hbar)}\mathcal{D}x(\tau)$ is a closed integration over the paths $x(\tau)$, $\tau$ is the Euclidean or imaginary time, and $V[x(\tau)]$ is the potential energy. It is well known that, within this picture, the imaginary time paths correspond to the quantum mechanical spreading of the particle at a finite temperature, and that in the high-temperature limit this spreading mapped by the imaginary paths collapses towards a point (which is clearly the position of the classical particle). According to this analysis, Feynman indicated[1] that a classical-like description of a quantum system can be given by representing the paths in terms of their mean value or centroid, and their fluctuation from it, that is,

$$Z=\int \rho_c(x_c)dx_c=\int dx_c\int_{x(0)=x(\beta\hbar)}\mathcal{D}x\,\delta(x_c-x_0) \times\exp\left\{-\frac{1}{\hbar}S[x(\tau)]\right\}, \tag{3}$$

where

$$x_0=\frac{1}{\beta\hbar}\int_0^{\beta\hbar}x(\tau)d\tau \tag{4}$$

is the centroid of the imaginary time trajectory of a particle, and the path integral in Eq. (3) above defines the centroid density, $\rho_c(x_c)$. In this way, the centroid variable becomes the relevant variable from which to derive effective potentials that take into account the imaginary time path fluctuations of the quantum system at the specified temperature, and with it, all the equilibrium properties of the system, that is,

$$Z=\left(\frac{m}{2\pi\beta\hbar^2}\right)^{1/2}\int dx_c\exp\{-\beta V_{\mathrm{eff}}(x_c)\}, \tag{5a}$$

where

$$V_{\mathrm{eff}}=-\frac{1}{\beta}\ln[(2\pi\beta\hbar^2/m)^{1/2}\rho_c(x_c)]. \tag{5b}$$

Additionally, in the last decade Voth and co-workers[11,16,17] have extended Feynman's ideas by introducing the concept of centroid dynamics and providing the means to evaluate quantum mechanical real-time correlation functions. They have shown, by using the phase space representation of the path integral centroid theory,[17] that the centroid variables evolve according to a generalized Ehrenfest's theorem, i.e.,

$$\frac{dx_c(t)}{dt}=\frac{p_c(t)}{m} \quad \text{and} \quad \frac{dp_c(t)}{dt}=F_c(t), \tag{6}$$

where $x_c$ and $p_c$ are the position and momentum centroid, respectively. These equations of motion have a classical form, however, in general the centroid force, $F_c(t)$, is not a function of the position centroid at time $t$ only. The CMD approximation closes those relationships by approximating the centroid force as determined by the instantaneous position of the centroid, $F_c(t)\approx F_c[x_c(t)]$ (see Ref. 17 for details). Therefore, the CMD method implies the evaluation of the centroid forces according to an effective potential (defined by the centroid positions and the quantum imaginary time path fluctuations), and the classical evolution of the centroid positions according to Eqs. (6).

In practice, however, the centroid force is evaluated with a molecular dynamics (or Monte Carlo) algorithm using the discrete representation of the continuous imaginary paths.[2,11] In the discretized path integral picture the centroid variable $x_0$ [see Eq. (4)], becomes the center of mass of the isomorphic polymer of $P$ classical quasiparticles (or beads) such that,[11]

$$x_0=\frac{1}{P}\sum_{t=1}^{P}x_t. \tag{7}$$

This discretization parameter is chosen such that the calculation is sufficiently well converged to the $P\to\infty$ limiting result.

In order to carry out the path integral evaluation via molecular dynamics a hamiltonian is required. (As will be seen later in this paper, the evaluation of the constrained path integral via MD is easily generalized to the rotational case.

The Monte Carlo approach will also be discussed briefly). For a discretized quantum particle, a Hamiltonian can be defined as[2]

$$H=\sum_{t=1}^{P}\left[\frac{p_t^2}{2m_t'}+\frac{mP}{2\hbar^2\beta^2}(x_t-x_{t+1})^2+\frac{1}{P}V(x_t)\right], \tag{8}$$

where $p_t$ and $x_t$ are the momenta and positions of the beads, respectively. The kinetic term is completely arbitrary, the second term is the potential due to nearest-neighbor harmonic coupling between beads that arises from the free particle part of the density matrix (this term is strictly of quantum origin), and the last term is the interaction due to the external intermolecular potential. Thus, we define the force acting on the bead $t$, $F_t^{\text{bead}}$, as $F_t^{\text{bead}}=F_t-F_c$, where $F_t$ is the total force acting on this bead [associated with the quantum and intermolecular potentials identified in Eq. (8)] and the centroid force $F_c$ is defined by

$$F_c=\frac{1}{P}\sum_{t=1}^{P}F_t. \tag{9}$$

By implementing the constraint $\Sigma_{t=1}^{P}p_t=0$, and since by definition $\Sigma_{t=1}^{P}F_t^{\text{bead}}=0$, a calculation of the centroid force $F_c$ is easily carried out while the centroid, or ''beads' center-of-mass,'' will be a conserved quantity in the dynamics.[18]

### B. CMD for rigid bodies

The discussion presented above can be extended to the treatment of a collection of rigid objects. For present purposes it is sufficient (although not necessary) to assume that these bodies posses a classical-like mass but a relatively small (quantum-like) inertia moment at a certain finite temperature. It is clear that the coordinates of any of these rigid objects can be specified by a (unique) center-of-mass position and a quantum (uncertain within a certain neighborhood) orientation. As a consequence, an effective potential can be defined by introducing the concept of an *orientational centroid* and by taking into account the (molecular) *orientational uncertainty* by analogy to the Cartesian develop. Thus, in view of the similarity in the physical meaning of the translational and rotational centroids, the calculation of equilibrium and dynamical properties can then be carried out by evaluating the centroid forces and centroid torques according to the CMD approximation. (Although, in general, a rotational imaginary time path could close into itself[19] such a phenomenon will effectively not occur in liquid water, as will be seen below.) However, the extension of the centroid methodology to rotations,[18] while initially appearing straightforward, also has several subtleties, not the least of which include the well-known noncommutativity property of finite rotations. Additionally, in resolving the problem, three frames will be required to describe rotations, the laboratory frame with respect to which the centroid moves, the centroid frame with respect to which the beads move, and the local frames of the beads.

Analogous to the translational case, a rotational Hamiltonian can be defined for a single quantum rotor in a classical potential as

$$H=\sum_{t=1}^{P}\left[\left\{\frac{L_{x,t}^2}{2I_x'}+\frac{L_{y,t}^2}{2I_y'}+\frac{L_{z,t}^2}{2I_z'}\right\}+\left\{\frac{IP\Gamma^2(t+1,t)}{2\hbar^2\beta^2}\right\}+\frac{1}{P}V(r,q_t)\right], \tag{10}$$

where the first (kinetic) term is, as before, arbitrary, the second term is of a quantum nature (and can be easily derived from the free orientational density matrix of a spherical top[3,20]), and the third term is due to the external classical potential which depends on the center-of-mass position ($r$) and the orientational coordinates (the quaternion, $q_t$). In the second term of Eq. (10) (generalized for three-dimensional rotations) the inertia moment is approximated by $I=\sqrt[3]{I_xI_yI_z}$, $\Gamma(t+1,t)=2\arccos(\chi_{t+1})$ represents the rotation angle (or arclength) between the beads $t+1$ and $t$, and $\chi_{t+1}$ is the scalar element of the composite quaternion between $q^t$ and $q^{t+1}$. $\chi_{t+1}$ can be calculated from

$$\chi_{t+1}=q_0^{t+1}q_0^t+q_1^{t+1}q_1^t+q_2^{t+1}q_2^t+q_3^{t+1}q_3^t, \tag{11}$$

where $q^t=(q_0^t,q_1^t,q_2^t,q_3^t)$ and $q^{t+1}=(q_0^{t+1},q_1^{t+1},q_2^{t+1},q_3^{t+1})$ are the quaternion parameters that specify the orientations of the beads $t$ and $t+1$, respectively.

The orientational centroid can be conserved dynamically by requiring the sum of the torques acting on the beads to be zero in the centroid frame,

$$\sum_{t=1}^{P}T_t^{\text{bead}}=0, \tag{12a}$$

and by imposing the initial constraint on the angular momentum sum in the centroid frame,

$$\sum_{t=1}^{P}L_t=0. \tag{12b}$$

The torque $T_{qu}$ (due to the harmonic orientational coupling between beads) acting on a particular bead $t$ can be expressed in quaternion form as

$$T_{qu}=T^{(t+1)}+T^{(t-1)}=\frac{2IP}{\hbar^2\beta^2}\times_t\left[\frac{\Gamma(t+1,t)}{\sqrt{1-\chi_{t+1}^2}}\left(\frac{\partial\chi_{t+1}}{\partial q^{t+1}}\right)+\frac{\Gamma(t-1,t)}{\sqrt{1-\chi_{t-1}^2}}\left(\frac{\partial\chi_{t-1}}{\partial q^{t-1}}\right)\right], \tag{13}$$

where the derivatives need to be evaluated considering the unitary constraint on the quaternions parameters (see Ref. 18 for details). Clearly, the total torque $T_t$ acting on the bead $t$ of a particular molecule will also include a torque $T_{\text{class}}$ due to the intermolecular orientational interaction, i.e., $T_t=T_{qu}+T_{\text{class}}$. Analogous to the translational case, we can define $T_t^{\text{bead}}=T_t-T_c$, where the centroid torque is

$$T_c=\frac{1}{P}\sum_{t=1}^{P}T_t. \tag{14}$$

Utilizing the torques $T_t^{\text{bead}}$ adduced above, in conjunction with the centroid constraint of Eq. (12b), a dynamics can be generated such that the ''orientational neighborhood'' is

sampled and the average centroid torque (and the centroid force) estimated. However, an important difference in relation to translational motion is that within the context of the finite-difference methods used to solve the equations of motion, finite rotations do not commute and a small error arises associated with the preservation of the orientational centroid. Therefore, as the bead dynamics proceed it is seen that the real centroid drifts slightly from the original or ideal orientational centroid.[18] This error can be eliminated by exploiting the geometric properties of the quaternion parameters together with the aid of a definition for the orientational centroid.

The question of how to enforce the conservation of the orientational centroid can be handled, without loss of generality, by letting the orientational centroid be the quaternion (1,0,0,0) and correcting the orientation of one bead in terms of the orientations of the remaining beads. The two-bead case is straightforward (since the beads are inverse quaternions of each other, $q_2 = q_1^{-1}$) and the three-bead case has been recently solved in Ref. 18. Thus, iterative procedures based on the two-bead and three-bead expressions are easily implemented for an arbitrary number of beads. Such a procedure can then be used in addition to the dynamical constraint on the torques described above [see Eq. (12)] to guarantee conservation of the centroid during the integration of the beads' equations of motion. It should be clear at this point that the above procedure could also be utilized in a Monte Carlo algorithm to determine sets of bead quaternions that satisfy the centroid, thereby providing an alternate means for the evaluation of the constrained path integral.

A final concern involves the definition of the orientational centroid. The orientational centroid can be defined[18] as that orientation $q_c$ that satisfies,

$$\min\left[\sum_{t=1}^{P} \Gamma^2(q_c, q_t)\right], \tag{15}$$

where $\Gamma(q_c, q_t)$ is the rotation angle (or arclength) between the centroid orientation and the orientation of bead $t$, $q_t$. With this definition one can obviously find the centroid of a set of orientations through a Monte Carlo search that exploits this minimization condition as a criterion for rejection/acceptance of trial centroid moves. Convergence is then achieved by finding that trial centroid that can no longer be improved. Such a search procedure also allows one to confirm centroid conservation at any stage of a CMD simulation. Other minimization algorithms designed to average quaternions have also been published recently.[21] It is interesting to note that a similar minimization algorithm could be implemented for the determination of the translational centroid; however, it is much easier to find analytically by using Eq. (7). Unfortunately, an analytical definition for the orientational centroid is not known.

## III. SIMULATION DETAILS

Classical molecular dynamics simulations were performed for liquid water at 25 °C. A Gaussian thermostat was used to control the temperature of 256 molecules that interact through the TIP4P (Ref. 8) pair potential at a constant density of 0.998 g/cm. The Ewald summation technique[22] with a truncated octahedron simulation cell was utilized in combination with periodic boundary conditions. The equations of motion were integrated using a fourth order Gear predictor corrector algorithm,[22] in which the rotational degrees of freedom were represented with quaternions.[23] Quantum simulations were performed under the same conditions with the additional bead dynamics controlled with a separate Nosé-Hoover chain thermostat[24] for each bead and the appropriate bead constraints. The time steps used in the classical and quantum simulations were of 1 fs and 0.125 fs, respectively. The imaginary time dynamics was carried out with a time step of 0.5 fs with inertia moments (for each axis) on each bead twice that of the real molecule. The classical and quantum simulations were equilibrated for 0.1 ns and averaged for 0.5 ns.

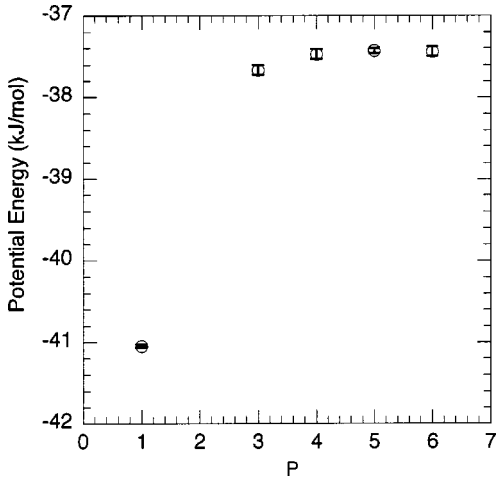


FIG. 1. Convergence of the intermolecular potential energy of the liquid $H_2O$ system as a function of the path integral discretization number $P$.

The convergence, with respect to $P$, in the quantum simulations of liquid water is very clearly seen in the average interaction energies presented in Fig. 1 (where the value of $P=1$ is the classical result). It is important to have demonstrated convergence particularly when examining isotopic effects in quantum simulations. In Fig. 1, we have included an error bar for each value. Although the values for $P=3$ and 4 account for a significant part of the quantum effect, convergence is only attained for $P=5$ and 6 where intermolecular potentials are the same within the statistical error. Further evidence of the convergence of the results with respect to $P$ is obtained by checking other equilibrium and dynamical properties of the liquid. Figure 2 shows the convergence of the oxygen-hydrogen radial distribution function for simulations carried out with values of $P=3$, 4, 5 and 6. The simulation with $P=3$ differs only slightly (shifted towards more classical behavior) from the results for $P=4$, 5, or 6, which are otherwise indistinguishable. Figure 3 shows the similarity in the translational and rotational velocity time correlation functions for $P=4$, 5, and 6, where again the curves for $P=3$ (not shown in this figure) demonstrate slightly shifted behavior. From this analysis we can conclude that the use of a value of $P=5$ for the discretization parameter provides converged results in the present quantum simulations. It is

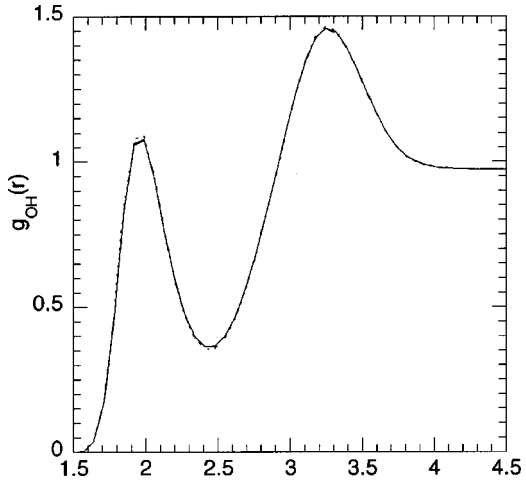


FIG. 2. Convergence of the oxygen-hydrogen radial distribution function of quantum liquid $H_2O$ with respect to the value of the discretization parameter $P$. The results represented by a dotted line, dashed line, dot-dashed line, and solid line correspond to the values $P=3$, 4, 5, and 6, respectively.

important to note that in previous equilibrium PIMD calculations of Rossky and co-workers[5] with rigid water models, convergence was also observed with $P=5$. We also remark that this relatively low value of convergence with $P$ is one of the assets of the present rigid-body approach; the value of $P$ for the quantum description of the hydrogen in water is typically more than 20 (Refs. 6 and 12) (Ref. 10 is an exception to this since $P$ was set to 16, however, convergence was not demonstrated).

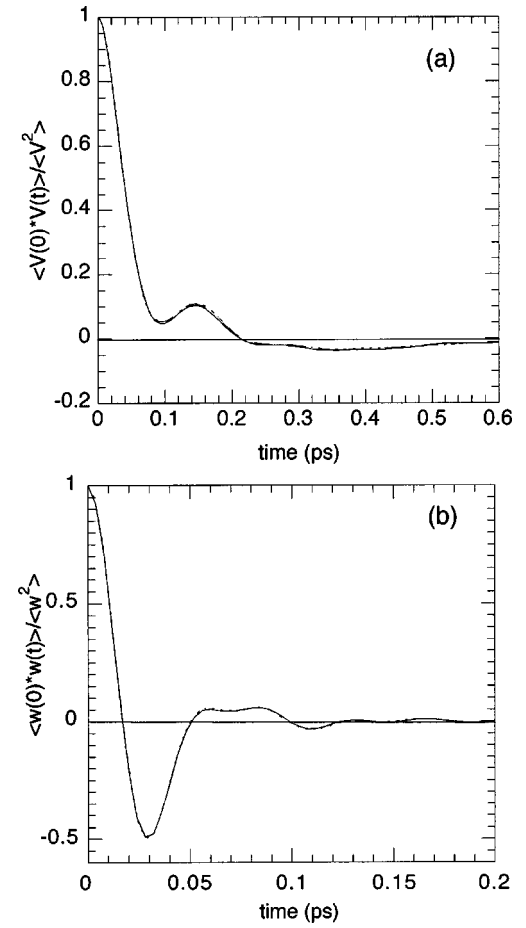


FIG. 3. Behavior of (a) the linear velocity and (b) the angular velocity time correlation functions for different values of the discretization parameter $P$. The dotted line, the dashed line, and the solid line correspond to the values $P=4$, 5, and 6, respectively.

There are essentially two ways to evaluate path integrals via molecular dynamics coupled with the centroid evolution.[25] In the *primitive algorithm*, the centroids have a classical-like time step and are only propagated further once sufficiently well-converged averaged (centroid) forces and torques have been accumulated; in the *adiabatic approach*, a very small centroid (real) time step is used together with very small bead masses (relative to the real centroid mass) such that the beads move much faster than the centroid. The adiabatic approach is significantly more efficient and is usually implemented[25] on suitable coordinates that uncouple the centroid motion and the bead motion (normal coordinates). In the present study, a ''quasiadiabatic'' approach has been chosen. In this approach a small number of steps in imaginary time are performed for every small centroid time step.[12] A number of tests to address its reliability have been carried out. A centroid time step significantly smaller than the usual classical time step (0.125 fs) was chosen and several values for the number of imaginary time steps were tested. It is clear that the results should be independent of the number of imaginary time steps performed at each real time step provided that a small enough real time step has been chosen and that convergence (in the adiabatic sense) of the centroid forces and centroid torques has been achieved. It was found that structural functions such as $g_{\text{O-H}}(r)$, or the average energies, are unchanged by the use of 3 or 5 imaginary steps (this explicit comparison is not shown). A more challenging test is perhaps in the dynamical properties; results for the linear velocity and angular velocity autocorrelation functions are shown in Fig. 4. The results obtained with 3 or 5 imaginary steps are identical within the estimated errors. As a consequence, three imaginary time steps were used for each real time step in all remaining simulations. We remark that testing utilizing the primitive algorithm (with 300 imaginary steps per regular centroid step) confirmed the validity of our quasiadiabatic implementations of CMD.

## IV. RESULTS AND DISCUSSION

### A. Equilibrium properties

The oxygen-oxygen and oxygen-hydrogen radial distribution functions were calculated for $H_2O$ and $D_2O$ via classical MD and rigid-body CMD techniques; they are presented in Figs. 5 and 6. These structural functions, as determined from classical molecular dynamics, are essentially identical for $H_2O$ and $D_2O$, thus we have chosen not to include the classical $D_2O$ radial distribution results. Figure 5 compares the oxygen-oxygen radial distribution functions for classical $H_2O$ and quantum $H_2O$ and $D_2O$. As expected, the quantum $H_2O$ is the least structured and the classical $H_2O$ ($D_2O$) is the most structured, while the quantum $D_2O$ result lies in between. Hence, it is clear that as the system becomes more quantum mechanical, there is effectively a softening of the structure with diminished peaks and raised

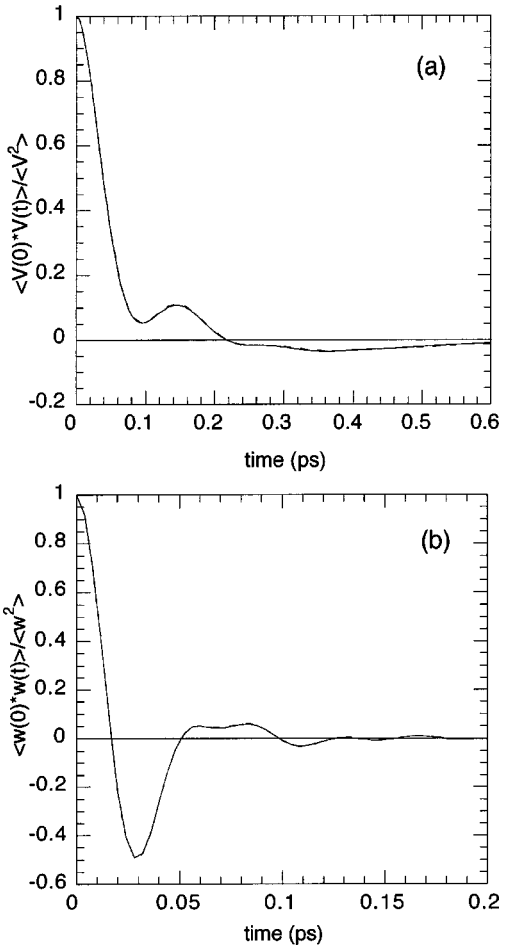


FIG. 4. Convergence of the linear velocity time correlation function (a) and the angular velocity time correlation function (b) for different numbers of quantum steps per centroid time step. In both graphs, the solid line and the dashed line correspond to 3 and 5 quantum steps, respectively.

valleys. This trend agrees with previous quantum simulation results performed on either flexible[4,6,12] or rigid water models,[3,5] although the present results exhibit much better convergence (as can be seen in the inset of Fig. 5), presumably, due to the longer length of real time simulation. The

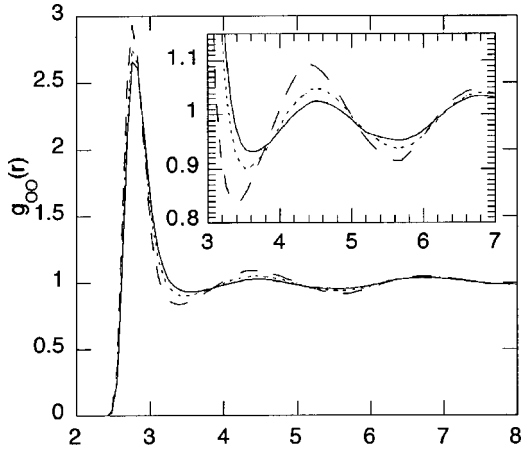


FIG. 5. Oxygen-oxygen radial distribution function for the three systems: classical water (dashed line), quantum $H_2O$ (solid line), and quantum $D_2O$ (dotted line), all at ambient conditions.

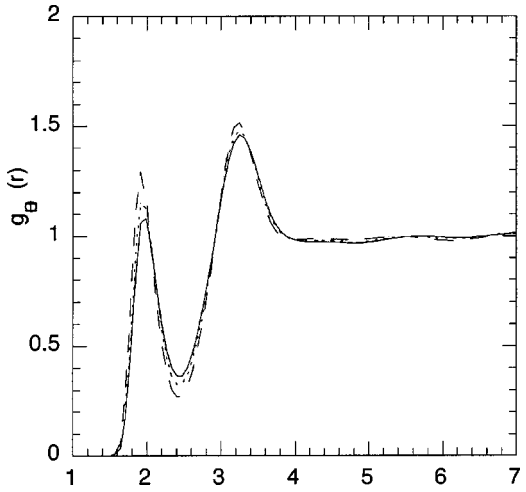


FIG. 6. Oxygen-hydrogen radial distribution function for the three systems: classical water (dashed line), quantum $H_2O$ (solid line), and quantum $D_2O$ (dotted lined).

oxygen-hydrogen radial distribution functions, shown in Fig. 6, confirm this interpretation. The peak at 1.9 Å, associated to the hydrogen bond, clearly shows that classical $H_2O$ water exhibits the strongest hydrogen bonding, followed by the quantum $D_2O$ and quantum $H_2O$ liquids, respectively. The agreement between these results and previous simulations using flexible models confirms the previous observation[5] that most of the quantum effect in water comes from rotational uncertainty. Furthermore, the agreement between the present results and previously reported PI simulations with rigid water models reaffirms a very important property of CMD, that of generating equilibrium averages if the system is ergodic.[17] We remark that the simulations presented here are carried out with a centroid orientational constraint, while those of Rossky and co-workers[3,5] utilized rigid-body quantum simulations where nonconstrained path integrals were evaluated.

The apparent softening of the intermolecular interactions found in the quantum simulation results presented above (using a rigid model approximation) appears as a consequence, exclusively, of the effect of quantum mechanics upon molecular orientations. In Fig. 7 probability distributions as mapped by the rigid-body CMD methodology are shown representing the quantum mechanical rotational uncertainty of light and heavy water molecules in their liquids. In this figure the symbols represent explicit data points, while the continuous lines represent fits of these points to the expected Gaussian behavior. The tails of the probability distributions are expanded in the inset with a logarithm scale. As expected, the $H_2O$ molecule has a significantly larger orientational uncertainty than the $D_2O$ molecule, and this leads to an increased softening of the effective intermolecular potential for $H_2O$ in relation to $D_2O$. The average orientational uncertainties (calculated as twice the average rotation angle between the beads and the centroid) of the $H_2O$ and $D_2O$ molecules are 11.3° and 8.9°, respectively, which is somewhat smaller than the value derived from the estimated de Broglie wavelength (~0.3 Å of a free proton) at room temperature. It is also apparent, from Fig. 7, that the probability

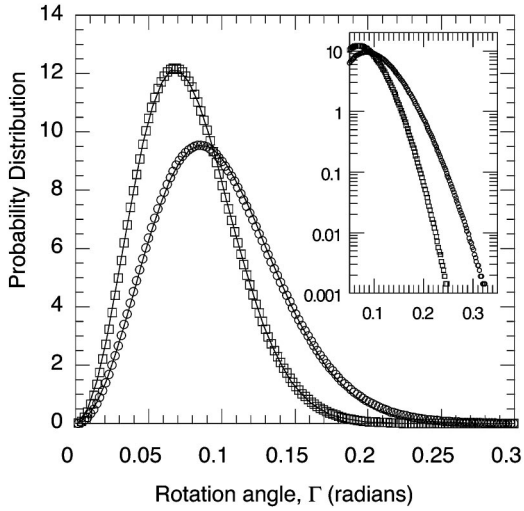


FIG. 7. Normalized probability distribution of the bead-centroid rotation angle. The circles and squares correspond to the liquid $H_2O$ and liquid $D_2O$ systems, respectively.

of finding an angle between any bead and the centroid larger than $\pi/2$ (90°) is effectively zero, which is a requirement for the existence of a unique *rotational centroid* in the present approach.[18]

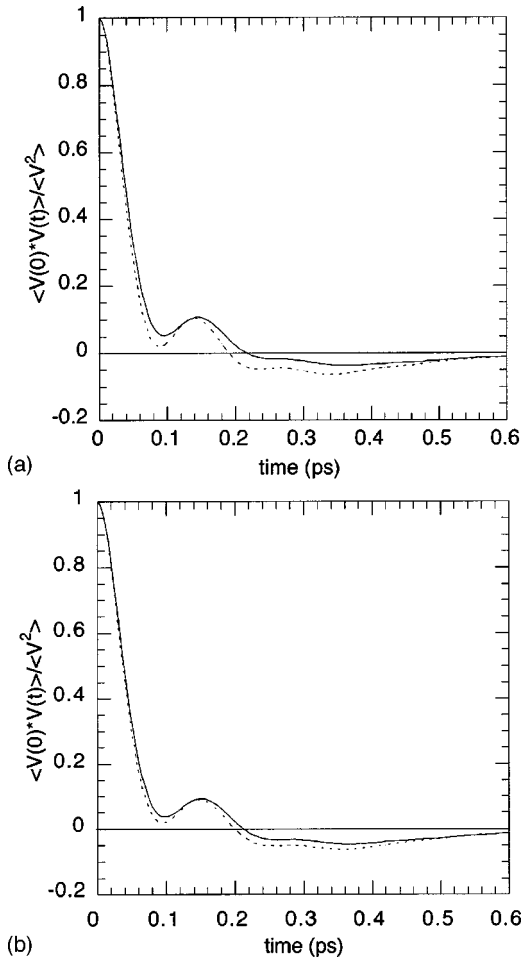


FIG. 8. Linear velocity time correlation functions of classical and quantum (a) $H_2O$ and (b) $D_2O$. The dashed line corresponds to the classical result and the solid line corresponds to the quantum result.

In Table I we report values of the potential energies obtained in the present classical and quantum simulations and compare them with previous calculations. The relative change in the potential energy due to the rotational quantization for the $H_2O$ and $D_2O$ systems is 8.8% and 5.9%, respectively. It can be clearly seen that the classical-to-quantum shift in energy for light water is essentially identical to the relative changes found by Lobaugh and Voth using the CMD methodology in an atomic approach on a flexible model.[12] Our relative changes for $H_2O$ and $D_2O$, however, are somewhat larger than those reported by Rossky and co-workers.[5] It is worth mentioning that the energy difference between the quantum $D_2O$ and quantum $H_2O$ simulations is 1.2 kJ/mol, and this result is very close to the difference in the experimental heats of vaporization of $D_2O$ and $H_2O$ (1.4 kJ/mol, Ref. 12). Finally, it is worth noting that although a very recent first-principles study has reported that the ''softening'' observed above is apparently compensated by an increase in the molecular dipole moment,[10] the extent of this balance, is not known quantitatively nor is the relationship between their energies and the experimental heats of vaporization.

### B. Dynamical properties

Since the translational degrees of freedom have not been quantized, the translational dynamical information of the present quantum simulations is immediately available from the centroid time correlation function. The velocity time autocorrelation function for classical and quantum $H_2O$ and $D_2O$ systems is presented in Fig. 8. It is apparent that there is a significant difference between the classical and the quantum results of liquid $H_2O$ [see Fig. 8(a)]. The principal changes seen in this function are the loss of structure (i.e., a dampening of the oscillatory behavior) and a shift of the maxima and minima to longer times for the quantized systems with respect to the classical simulation result. These differences are consistently smaller in the $D_2O$ system, although still noticeable [see Fig. 8(b)]. In order to interpret this effect, we remark that the principal intermolecular forces in water (hydrogen bond interactions) are very directional, but in the quantum system the forces are averaged over the molecular rotational uncertainty. These averaged (or centroid) forces are smaller than the classical ones, and consequently they generate a more strongly dampened velocity time correlation function with maxima and minima shifted towards longer times. Hence, the quantum system is not only less structured in space (as discussed above) but is also less correlated in time in comparison with the classical system. We have also observed that for the Cartesian components of the velocity time correlation function (not shown) each of the individual *x*, *y*, or *z* components of the velocity time correlation function experience such ''softening''; however, there is no evidence of this shift being particularly larger in any specific direction.

Table II presents the translational self-diffusion coefficients and their local frame components obtained for the classical and quantum simulations of light and heavy liquid water through the well-known relationships,[22,26]

TABLE I. Intermolecular potential energies obtained in the classical and quantum simulations in kJ/mol.

| | | Quantum | | Relative shift (%) | |
|---|---|---|---|---|---|
| | Classical | $H_2O$ | $D_2O$ | Class/$H_2O$ | Class/$D_2O$ |
| This work | 41.05±0.02 | −37.43±0.02 | −38.63±0.02 | 8.8 | 5.9 |
| TIP4P[a] | −41.9 | −39.1 | −39.9 | 6.7 | 4.8 |
| SPC[a] | −42.7 | −39.7 | −40.5 | 7.0 | 5.2 |
| SPC/F[b] | −47.51±0.04 | −43.69±0.06 | ⋯ | 8.0 | ⋯ |
| SPC/$F_2$[b] | −49.44±0.04 | −45.36±0.05 | ⋯ | 8.2 | ⋯ |
| MCDHO[c] | −47.40±0.08 | −41.0±0.4 | ⋯ | 13.5 | |

[a]Reference 5.
[b]Reference 12.
[c]Reference 6.

$$D_\alpha = \int_0^\infty \langle [\mathbf{v}_\alpha(0)\cdot\mathbf{e}_\alpha(0)]\cdot[\mathbf{v}_\alpha(t)\cdot\mathbf{e}_\alpha(0)]\rangle dt, \tag{15a}$$

and

$$D = \tfrac{1}{3}\sum_\alpha D_\alpha, \tag{15b}$$

where $\mathbf{e}_\alpha$ are the unit vectors of the principal frame ($\alpha = x,y,z$) and $\mathbf{v}_\alpha(t)\cdot\mathbf{e}_\alpha(0)$ is the $\alpha$ component of the linear velocity of the center of mass defined in the local frame at $t=0$. The local frame is defined such that the $z$ axis lies along the axis of symmetry and $x$ axis is in the plane of the molecule. As can be seen from Table II the quantum self-diffusion coefficients are, as expected, larger than the classical values, the effect being most pronounced for light water. The discrepancy between the absolute values and the experimental results are due to the TIP4P parametrization of the water-water interaction which, even classically, overestimates the self-diffusion coefficients. We note, however, that the isotopic ratio of the self-diffusion coefficient from the quantum calculations is significantly closer than the corresponding classical value to the experimental isotopic ratio, which implies that the quantum simulations much more accurately capture the differences between the dynamics of $H_2O$ and $D_2O$. The isotopic ratio obtained from our classical simulations with the TIP4P potential are in excellent agreement with that previously obtained for the SPC/E model,[26] confirming the inability of classical dynamics to capture isotopic effect in liquid water.

The effect of quantization given as the ratio $D^{\text{quan}}_{H_2O}/D^{\text{class}}_{H_2O}$ is in very good agreement with previously reported results from CMD simulations. The ratio $D^{\text{quan}}_{H_2O}/D^{\text{class}}_{H_2O}$ of 1.7±0.8 reported by Lobaugh and Voth[12] is statistically indistinguishable from the present value of 1.53±0.09. We note that Guillot and Guissani[13] also found a ratio of 1.7, but have not reported error bars. It is important to emphasize that the roughly 50% increase in the translational diffusion constant, when going from classical to quantum dynamics (for liquid $H_2O$), is very significant taking into account that this effect is an indirect consequence of the quantization (in the sense that is the rotational and not the translational motion that has been treated quantum mechanically). The fact that the orientational quantization is found to have a significant impact on the translational dynamics is clearly a consequence of the strong coupling between the rotational and translational motions of water molecules in the liquid.

In order to determine angular-velocity quantum time correlation functions, we recall that the CMD approach offers the possibility of extracting approximated quantum correlation functions, $\langle A(t)A(0)\rangle$, from the centroid correlation function, $\langle A^{(c)}(t)A^{(c)}(0)\rangle$, which can be accumulated during the simulation. These two correlation functions are related in frequency space by[12,16,17]

$$I(w) = (\hbar w/2)[\coth(\hbar w/2)+1]I^{(c)}(w), \tag{16}$$

where $I(w)$ and $I^{(c)}(w)$ are the Fourier transforms of the quantum and centroid correlation functions, respectively. In Fig. 9 we show the components of the angular velocity time correlation function of liquid $H_2O$ as obtained from classical and quantum simulations. In the $x$ component, we see a shift of the maxima and minima in the quantum correlation function towards longer times with respect to the classical. In the

TABLE II. Translational self-diffusion coefficients in $10^5$ $cm^2/s$ for TIP4P liquid water at 25 °C. The errors of the calculated values are about 1%. The experimental values are from Ref. 26.

| System | | $D$ | $D_x$ | $D_y$ | $D_z$ | Expt. |
|---|---|---|---|---|---|---|
| $H_2O$ | Class | 3.58 | 3.36 | 4.25 | 3.14 | 2.3 |
| | Quant | 5.48 | 5.18 | 6.51 | 4.74 | |
| $D_2O$ | Class | 3.45 | 3.22 | 4.14 | 2.98 | 1.9 |
| | Quant | 4.57 | 4.35 | 5.39 | 3.97 | |
| $H_2O/D_2O$ | Class | 1.04 | 1.04 | 1.03 | 1.05 | 1.21 |
| | Quant | 1.20 | 1.20 | 1.21 | 1.19 | |

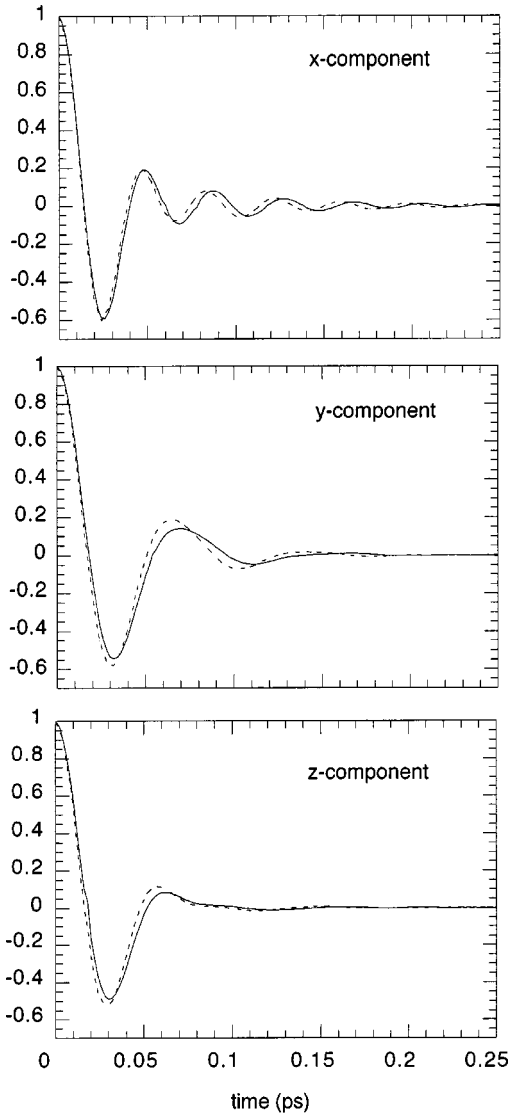


FIG. 9. The *x*, *y*, and *z* components of the angular velocity time correlation function obtained from classical (dashed line) and quantum (solid line) simulations of liquid $H_2O$.

*y* and *z* components, we additionally observe a very significant dampening of the oscillations in the quantum functions relative to the classical ones.

These observations are further clarified in Fig. 10 where we show the power spectra of two components of the angular velocity time correlation function. Since the *z* and *y* components (which are oriented along the dipole moment and perpendicular to the molecular plane, respectively) have similar time dependence (see Fig. 9), their power spectra have a similar shape and we have chosen to include only one of them. The power spectrum of the *x* component, which is associated with the smallest inertial moment, appears skewed towards higher frequencies while the *y* and *z* components have a more symmetric shape. The observed bands at about 700 and 500 $cm^{-1}$, which are due to the librational oscillations of the molecule in the liquid, are clearly shifted to lower frequencies in the quantum simulation. This shift to lower frequencies observed in the quantum simulation results is, obviously, a reflection of the slower oscillatory behavior

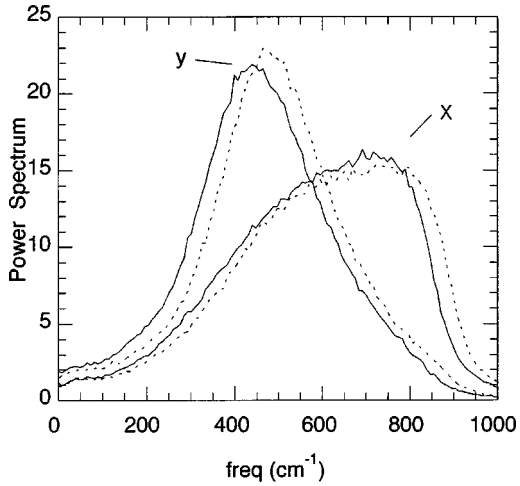


FIG. 10. Power spectra of the *x* and *y* components of the angular velocity time correlation function of liquid $H_2O$. The dotted lines correspond to the classical simulation and the solid lines correspond to the quantum simulation.

in the quantum time correlation functions in relation to the classical behavior, as seen in Fig. 9. The dampening of the oscillations of the *y* component of the quantum time correlation function (see Fig. 9) appears in Fig. 10 as a decrease in the intensity of the principal band in its power spectrum. These effects can again be associated with the apparent softening of the interaction potential as a consequence of the CMD averaging of the centroid torques, and as expected they were found to be smaller for $D_2O$ than for $H_2O$. The differences observed between the effects of quantization on the *x*, *y*, and *z* components of the angular velocity appear to be a consequence of the uneven impact of the softening within the (heterogeneous) local molecular environment. It is interesting to point out that direct use of the centroid angular velocity time correlation function instead of the approximate quantum time correlation function [obtained from Eq. (15)] does not change the above observations indicating that most of the effects of quantization are already captured directly with the classical-like evolution of the centroid (due to the effective centroid potential).

The single-molecule orientational autocorrelation functions, $C_1^z(t)$ and $C_2^z(t)$, defined as

$$C_k^z = \langle P_k[\vec{z}(t)\cdot\vec{z}(0)]\rangle, \tag{17}$$

where $\vec{z}$ is the *z* axis of the molecule (aligned with molecular dipolar vector) and $P_k$ denotes the Legendre polynomial of order *k*, were obtained from the present simulations of the liquid $H_2O$ and $D_2O$ systems. Spectral functions were calculated as

$$I_k^z = w^2\,\mathrm{Re}\int_0^\infty C_k^z(t)\exp(iwt)dt. \tag{18}$$

The functions $C_1^z(t)$, $C_2^z(t)$, $I_1^z(w)$, and $I_2^z(w)$ determined for the liquid $H_2O$ system are presented in Figs. 11 and 12. A significant increase of the rate of decay is observed in Fig. 11 in the time-domain behavior of $C_1^z(t)$ and $C_2^z(t)$ from the quantum simulations. A slight shift to longer times of the peak at about 0.1 ps is better resolved in the frequency do-

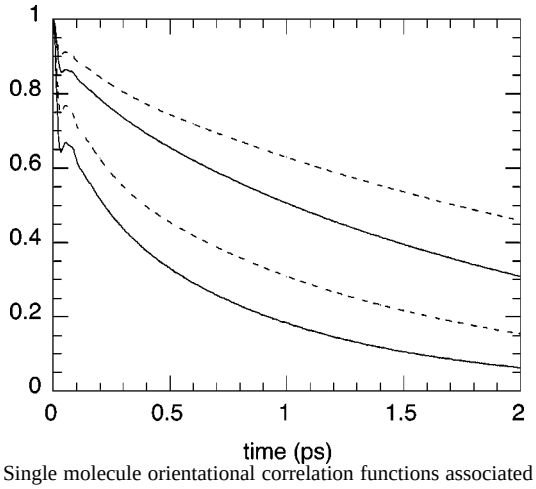


FIG. 11. Single molecule orientational correlation functions associated with the Legendre polynomial of order $k=1$ and $k=2$. The dashed line corresponds to the classical result and the solid line corresponds to the quantum result.

main spectrum of Fig. 12 as a shift to lower frequencies of the quantum result. The wide band located from 300 to 700 $cm^{-1}$ in Fig. 12 is characteristic of the molecular-librational motion of the molecular dipole in the liquid and has been previously reported in Raman experiments[27] and in classical simulation studies of light and heavy liquid water.[28] It is interesting to note that the shift observed here is somewhat similar to the one reported previously in classical simulations[28] and associated with an increase in the temperature of the liquid. The analogy between quantum effects and the effects of raising the temperature was made in the early simulation studies of the structure of quantum water.[3] In a forthcoming paper[29] we will examine in detail the level to which this analogy is valid in the equilibrium and the dynamical properties of liquid water. As expected, we also found the shift associated with the softening of the potential stronger within liquid $H_2O$ than in $D_2O$ in relation to their classical counterparts.

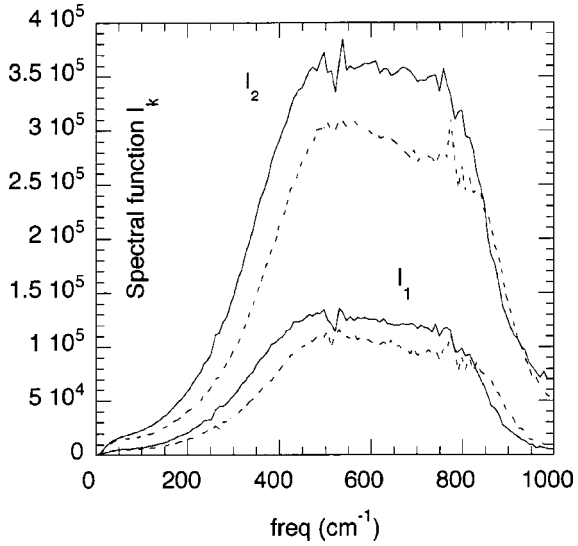


FIG. 12. The spectral functions $I_1$ and $I_2$. The dashed line represents the classical result and the solid line represents the quantum result.

TABLE III. Molecular and collective (dielectric) relaxation times (in ps) for TIP4P liquid water at 25 °C. Experimental values are from Ref. 26.

| System | | $\tau_1^z$ | $\tau_2^z$ | $\tau_D$ |
|---|---|---|---|---|
| $H_2O$ | Class | 2.79±0.03 | 0.952±0.005 | 7±1 |
| | Quant | 1.71±0.03 | 0.578±0.005 | 4±1 |
| | Expt. | ··· | ··· | 8.3 |
| $D_2O$ | Class | 3.16±0.03 | 1.073±0.005 | 7±1 |
| | Quant | 2.33±0.03 | 0.781±0.005 | 5±1 |
| | Expt. | ··· | ··· | 10.4 |
| $D_2O/H_2O$ | Class | 1.13 | 1.13 | 1.0 |
| | Quant | 1.36 | 1.35 | 1.2 |
| | Expt. | | | 1.26 |

From the quantum and classical orientational autocorrelation functions, $C_1^z(t)$ and $C_2^z(t)$, relaxation times can be calculated and compared. The single molecule orientational correlation times, or self-times, have been obtained by integrating the appropriate autocorrelation functions, i.e., $\tau_k^z = \int_0^{-\infty} C_k^z(t)dt$. In this study the orientational autocorrelation functions have been determined to sufficiently long times (2 ps) to allow the dominant contributions to $\tau_k^z$ to be obtained by direct numerical integration. The appropriate tail corrections to the self-times were evaluated by assuming a simple exponential decay in $C_k^z(t)$ at long times. The self-times values obtained, listed in Table III, are similar to those reported previously by other authors[12,26] and represent a further confirmation of the faster diffusive motion in a quantum liquid than in a classical one. For example, the ratio $(\tau_1^{z\,\mathrm{class}}/\tau_1^{z\,\mathrm{quant}})$ was reported by Lobaugh and Voth as 1.5±0.5 while in this study we have obtained extensively the same value, 1.6 ±0.07, where the considerable smaller errors bars arise from the much longer real-time trajectories of the present work. It is clearly seen from Table III that quantization sharply decreases the relaxation times for liquid $H_2O$, and it has a lesser impact in $D_2O$, as expected and in agreement with the results presented above.

The collective (or dielectric) relaxation times obtained from

$$\tau_D = \int_0^{\infty} \frac{\langle \mathbf{M}(t)\cdot\mathbf{M}(0)\rangle}{M^2} \tag{19}$$

for classical and quantum simulations of $D_2O$ and $H_2O$ are also presented in Table III. It can be again seen that the impact of rotational quantization is quite significant, especially in $H_2O$. While the absolute values obtained from the quantum simulations shift farther from the experimental results, the isotopic ratios calculated from the quantum simulations appear to approximate more closely the experimental isotopic ratio. However, the relatively large errors associated with these collective relaxation times make it difficult to draw any specific conclusions about the values of the ratios given in Table III. Nevertheless, the errors associated with the present results are considerably smaller than those of other quantum simulation studies.[12]

## V. CONCLUSIONS

In this paper we have discussed the application of the CMD methodology to systems of rigid bodies and we have implemented this technique to investigate liquid water at room temperature. Using a simple (rigid) water model, the TIP4P potential, we have systematically examined isotopic effects in the bulk properties of water. With this approach we have successfully reproduced results for the equilibrium and dynamical properties of light and heavy water as obtained from experiment and from previous path integral simulations.

Since this paper reports an initial study where CMD has been applied to the simulation of a model liquid system in which the molecules have been treated as rigid bodies, considerable attention was paid to the parametrization and characterization of the methodology. It was shown that the removal of the vibrational degrees of freedom, accompanied by the relatively low value of the discretization parameter ($P=5$) required for convergence, allow the present approach to be significantly (at least 20 times) faster than standard CMD. Additionally, its validity was confirmed by the fact that the rotational CMD technique recovers at a quantitative level essentially the full effect of quantization observed previously in quantum simulations with flexible models. This also implies that even within quantum dynamics, flexibility does not play a critical role in determining the bulk properties of liquid water. Furthermore, as a result of the considerably enhanced computational efficiency of the rigid-body CMD simulations, it was possible to generate significantly longer real-time trajectories with the accompanying reduction in the statistical errors in the properties of interest.

Explicit inclusion of the orientational degrees of freedom additionally allow a quantitative analysis of the rotational uncertainty of the $H_2O$ and $D_2O$ water molecules and its effect on the components of the angular velocity time correlation function. As expected, we have found a notably larger impact of quantization in $H_2O$ than in $D_2O$. Its influence on rotational dynamics, particularly librational motion and dipole relaxation times, is consistent with a ''softening'' of the intermolecular interactions. The enhancement of the linear self-diffusion coefficient (by roughly 50%) is an indirect effect of quantization and reflects the importance of rotational-translational coupling in the dynamics of liquid water.

This study confirms that, whereas classical simulations are unable to, quantum dynamical calculations can within a rigid-body approximation reproduce the known isotope effects in water. In future work we will use rigid-body CMD simulations to examine the temperature dependence of quantum effects in liquid water,[29] to investigate the coupling between quantization and the local structure surrounding a molecule,[30] and to explore quantum effects in ice.[31]

## ACKNOWLEDGMENT

We are grateful for the financial support of the Natural Sciences and Engineering Research Council of Canada.

[1] R. P. Feynman and A. R. Hibbs, *Quantum Mechanics and Path Integrals* (McGraw-Hill, New York, 1965); R. P. Feynman, *Statistical Mechanics: A Set of Lectures* (Addison-Wesley, Redwood City, CA, 1972).
[2] B. J. Berne and D. Thirumalai, Annu. Rev. Phys. Chem. **37**, 401 (1986); D. Chandler, in *Liquids, Freezing and Glass Transition*, edited by J. P. Hansen, D. Levesque, and J. Zinn-Justin (Norh-Holland, Amsterdan, 1991).
[3] R. A. Kuharski and P. J. Rossky, J. Chem. Phys. **82**, 5164 (1985).
[4] A. Wallqvist and B. J. Berne, Chem. Phys. Lett. **117**, 214 (1985).
[5] G. S. del Buono, P. J. Rossky, and J. Schnitker, J. Chem. Phys. **95**, 3728 (1991).
[6] H. A. Stern and B. J. Berne, J. Chem. Phys. **115**, 7622 (2001).
[7] F. H. Stillinger and A. Rahman, J. Chem. Phys. **60**, 1545 (1974).
[8] H. J. C. Berendsen, J. P. M. Postma, W. F. van Gunsteren, and J. Hermans, in *Intermolecular Forces*, edited by B. Pullman (Reidel, Dordrecht, 1981), p. 331.
[9] W. L. Jorgensen, J. Chandrasekhar, J. D. Madura, R. W. Impey, and M. L. Klein, J. Chem. Phys. **79**, 926 (1983).
[10] B. Chen, I. Ivanov, M. L. Klein, and M. Parrinello, Phys. Rev. Lett. **91**, 215503 (2003).
[11] G. Voth, in *Advances in Chemical Physics*, Vol. XCIII, edited by I. Prigogine and S. A. Rice (Wiley, New York, 1996); G. A. Voth, in *Theoretical Methods in Condensed Phase Chemistry*, edited by S. D. Schwartz (Kluwer Academic, Amsterdam, 2000).
[12] J. Lobaugh and G. A. Voth, J. Chem. Phys. **106**, 2400 (1997).
[13] B. Guillot and Y. Guissani, J. Chem. Phys. **108**, 10162 (1998).
[14] A. Wallqvist and R. D. Mountain, in *Reviews in Computational Chemistry*, Vol. 13, edited by K. B. Lipkowitz and D. B. Boyd (Wiley, New York, 1999); B. Guillot, J. Mol. Liq. **101**, 219 (2002).
[15] M. Allesch, E. Schwegler, F. Gygi, and G. Galli, J. Chem. Phys. **120**, 5192 (2004).
[16] J. Cao and G. A. Voth, J. Chem. Phys. **99**, 10070 (1993); **100**, 5093 (1994); **100**, 5106 (1994); **101**, 6157 (1994); **101**, 6168 (1994).
[17] S. Jang and G. A. Voth, J. Chem. Phys. **111**, 2357 (1999); **111**, 2371 (1999).
[18] L. Hernández de la Peña and P. G. Kusalik, Mol. Phys. (to be published).
[19] For a review on the use of path integrals in rigid rotors, see D. Marx and M. H. Müser, J. Phys.: Condens. Matter **11**, R117 (1999).
[20] L. S. Schulman, *Techniques and Applications of Path Integration* (Wiley, New York, 1981).
[21] S. R. Buss and J. P. Fillmore, ACM Trans. Graphics **20**, 95 (2001).
[22] M. P. Allen and D. J. Tildesley, *Computer Simulation of Liquids* (Oxford University Press, New York, 1989).
[23] D. J. Evans and S. Murad, Mol. Phys. **68**, 6 (1989); D. J. Evans, *ibid.* **34**, 317 (1977); D. J. Evans and S. Murad, *ibid.* **34**, 327 (1977).
[24] G. J. Martina and M. L. Klein, J. Chem. Phys. **97**, 2635 (1992).
[25] M. Pavese, S. Jang, and G. A. Voth, Parallel Comput. **26**, 1025 (2000).
[26] I. M. Svishchev and P. G. Kusalik, J. Phys. Chem. **98**, 728 (1994).
[27] M. Mizoguchi, Y. Hori, and Y. Tominaga, J. Chem. Phys. **97**, 1961 (1992).
[28] I. M. Svishchev and P. G. Kusalik, J. Chem. Soc., Faraday Trans. **90**, 1405 (1994).
[29] L. Hernández de la Peña and P. G. Kusalik (unpublished).
[30] L. Hernández de la Peña and P. G. Kusalik (unpublished).
[31] L. Hernández de la Peña, M. S. Gulam Razul, and P. G. Kusalik (unpublished).